JCTC Journal of Chemical Theory and Computation

ARTICLE

pubs.acs.org/JCTC

Accurate Molecular Crystal Lattice Energies from a Fragment QM/MM Approach with On-the-Fly Ab Initio Force Field Parametrization

Shuhao Wen and Gregory J. O. Beran*

Department of Chemistry, University of California, Riverside, California 92521, United States

Supporting Information

ABSTRACT: We combine quantum and classical mechanics in a fragment-based many-body interaction model to predict organic molecular crystal lattice energies. Individual molecules in the central unit cell and their short-range pairwise interactions are modeled quantum mechanically, while long-range pairwise and many-body interactions are approximated classically. The classical contributions are evaluated using an accurate ab initio force field that is constructed on-the-fly from quantum mechanical calculations on the individual molecules in the unit cell. The force field parameters include ab initio distributed multipole moments, distributed polarizabilities, and isotropic two- and three-body atomic dispersion coefficients. This QM/MM fragment model reproduces full periodic MP2 lattice energies to within a couple kJ/mol at substantially reduced cost. When high-level electronic structure methods are coupled with the ab initio force field, molecular crystal lattice energies are predicted to within 2 kJ/mol of their experimental values for six of the seven crystals examined here. Finally, Axilrod−Teller−Muto three-body dispersion energy plays a nontrivial role in several of the molecular crystals studied here.

1. INTRODUCTION

Organic molecular crystals play a fundamental role in pharmaceuticals, agrochemicals, pigments, dyestuffs, foods, explosives, and organic electronic materials. Molecular crystal properties are strongly affected by the crystal packing. Multiple crystal packing arrangements, or polymorphs, are often thermodynamically accessible in real crystals and can have major real-world consequences.[1]

For example, a change in the crystal packing of rubrene, a promising organic semiconductor material, utterly destroys its high charge-carrier mobility.[2] Or consider that the appearance of a low-solubility polymorph of ritonavir, an anti-HIV drug, forced its temporary removal from the market. This prevented patients from receiving treatment and cost its maker an estimated $250 million in lost sales.[3] Clearly, substantial scientific and financial interest lies in knowing the structures and the properties of stable crystal polymorphs.

Over the past decade, substantial progress has been made toward the dream of predicting molecular crystal structures starting from only a single molecule, as evidenced by recent major improvements in the results of the blind crystal structure prediction tests.[4,5] Two advances instrumental to this progress are the development of robust, anisotropic force fields that include distributed multipolar expansions of the molecular charge distribution, induction, and dispersion[6,7] and the application of quantum mechanical models to crystal structure prediction, either to help determine intramolecular conformations or for fully periodic density functional theory (DFT) calculations.[6,8−16]

Unfortunately, traditional density functionals suffer from well-known difficulties in describing van der Waals dispersion interactions,[17,18] which are critical to modeling intermolecular interactions in molecular crystals. A number of strategies to correct this deficiency have been adopted, ranging from empirical corrections to the development of nonlocal density functions.[19−23] These techniques often work extremely well for molecular crystals, but counter-examples also exist.[24,25]

Moreover, the energy spacing between crystal polymorphs can be as little as 1 kJ/mol or less.[24,26] Differences among the lattice energy predictions from various density functionals often exceed this threshold. The absence of a clear strategy for systematically improving DFT calculations makes robust predictions difficult. Recent developments in periodic Møller−Plesset perturbation theory (MP2) are also very promising for crystal structure modeling,[27−32] but those calculations remain relatively computationally expensive.

The past few years have seen considerable interest in strategies that model molecular crystals through a hierarchical[33,34] or fragment-based scheme. The advantage of fragment-based models is that one can systematically improve the quality of the electronic structure method used to describe the fragments and their interactions. Many of these models, such as the fragment molecular orbital method,[35] are based on the many-body interaction expansion. The key distinguishing features between such methods lie in how they handle the long-range two-body (interactions between a pair of molecules) and the many-body (involving three molecules or more) contributions.

The most straightforward approach would be to simply neglect these terms, but they contribute too much to ignore. Long-range and many-body contributions typically account for ∼5−10% of the lattice energy, but they can contribute as much as ∼25%! One can do better if three-body terms are included explicitly, as has been demonstrated with highly accurate symmetry-adapted perturbation theory (SAPT) calculations, for example.[36,37] Unfortunately, the steep computational scaling of most electronic structure methods makes the explicit inclusion of three-body terms costly.

Received: August 2, 2011
Published: October 20, 2011

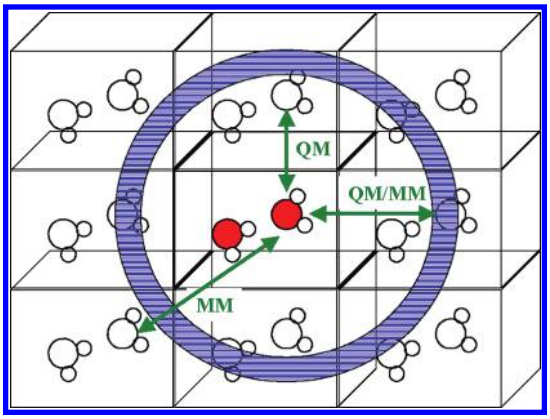

Figure 1. Pictorial representation for the treatment of two-body terms in periodic HMBI. Short-range dimers interactions are modeled quantum mechanically, while long-range ones are treated classically (MM). A linear combination of QM and MM is used in the blue region to transition smoothly between the two regimes.

The fragment molecular orbital method and related approaches incorporate many-body electrostatic induction effects via the use of an embedding potential in the one- and two-body terms.[38−42] However, this embedding potential complicates the evaluation of the nuclear derivatives required for structure optimization.[39,43] Alternatively, one can approximate the long-range/many-body terms in some fashion. A number of groups have used Hartree−Fock (HF) or DFT to capture these effects.[44−48] Both methods capture the many-body induction effectively, but they become computationally expensive for large unit cells. Both of these approaches have traditionally omitted many-body dispersion effects, which are sometimes important.

In our approach, quantum mechanics (QM) is used to treat the short-range interactions, while a polarizable force field (MM) is used to approximate the long-range two- and many-body interactions.[25,49,50] This hybrid QM/MM many-body interaction (HMBI) model differs from conventional QM/MM models in that it partitions different classes of interactions as either QM or MM based on their importance in the many-body interaction expansion, rather than by defining specific QM and MM regions of space.

We have recently demonstrated that this hybrid model enables the prediction of several small-molecule crystal lattice energies to within 4−5 kJ/mol, so-called chemical accuracy.[25] However, chemical accuracy is probably insufficient to discriminate among crystal polymorphs separated by only a kJ/mol or less. That earlier work used the Amoeba polarizable force field for the MM portion of the model. In this paper, we demonstrate that even better results are obtained when we replace the Amoeba forcefield with a high-quality ab initio force field whose parameters are calculated "on-the-fly" via separate electronic structure calculations performed for each molecule in the crystal unit cell.

Like our earlier work on molecular clusters,[50] this force field includes electrostatic and induction effects based on distributed multipole moments and polarizabilities. Here, we augment those terms with atomic dispersion coefficients to describe long-range two-body dispersion and Axilrod−Teller−Muto three-body dispersion. We also implement an Ewald summation-based treatment of multipolar electrostatics and induction for the periodic crystals (see also Supporting Information).

This force field model is analogous to those used in high-quality MM crystal modeling (e.g., refs 5, 7, and 51), with the force field parameters recalculated for each molecule/geometry to capture the variations in the properties (particularly multipole moments[5,50,51]) with geometry. No rigid monomer approximation is needed. Similar long-range terms are included in the "systematic fragmentation" model,[34] though the model described here differs in many details, including its use of a multipolar Ewald sum for long-range electrostatics, distributed polarizabilities, and the inclusion of three-body dispersion.

We demonstrate that this hybrid QM/MM approach reproduces periodic, fully quantum mechanical calculations to within a couple kJ/mol. More importantly, combining this ab initio force field with high-level electronic structure calculations reproduces experimental crystal lattice energies to within 2 kJ/mol for most of the crystals examined here. In other words, these predictions lie within the typical experimental error bars for molecular crystal lattice energies. Finally, we observe that the three-body Axilrod−Teller−Muto dispersion contribution is surprisingly important, even in some crystals where many-body induction would normally be expected to dominate.

2. THEORY

2.1. Periodic Hybrid Many-Body Interaction Model. The details of our hybrid QM/MM fragment approach for both clusters[49,50] and periodic systems[25] have been given previously, so we provide only a brief summary here. This fragment method decomposes a system into interacting molecules using a many-body interaction expansion. The intramolecular interactions and the most important intermolecular interactions are modeled quantum mechanically, while weaker intermolecular interactions are approximated classically. Specifically, for an infinite periodic molecular crystal, individual molecules in the central unit cell and shorter-range pairwise interactions are modeled quantum mechanically, while longer-range two-body interactions and all many-body interactions are treated using a polarizable force field (see Figure 1):

$$E_{\mathrm{PBC}}^{\mathrm{HMBI}} = E_{\mathrm{PBC}}^{\mathrm{MM}} + \sum_i (E_i^{\mathrm{QM}} - E_i^{\mathrm{MM}}) + \sum_{ij} d_{ij}^{\mathrm{smooth}} (\Delta^2 E_{ij}^{\mathrm{QM}} - \Delta^2 E_{ij}^{\mathrm{MM}}) + \frac{1}{2} \sum_i \sum_{\tilde{k}}^{\mathrm{images}} d_{i\tilde{k}}^{\mathrm{smooth}} (\Delta^2 E_{i\tilde{k}}^{\mathrm{QM}} - \Delta^2 E_{i\tilde{k}}^{\mathrm{MM}}) \quad (1)$$

Here, i and j run over molecules in the central unit cell, while $\tilde{k}$ runs over all periodic image molecules within some cutoff distance of molecule i, E_i corresponds to the energy of monomer i, and $\Delta^2 E_{ij}$ is the interaction energy between monomers i and j. Both can be calculated either quantum mechanically (QM) or with a force field (MM). $E_{\mathrm{PBC}}^{\mathrm{MM}}$ refers to the force field energy of the entire periodic crystal. To ensure smooth and continuous potential energy surfaces, the transition from short-range quantum to long-range classical treatments is spread over a finite region using a smoothing function d_{ij}^{smooth} that decays from 1 at radius r_1 to 0 at radius r_0:[52]

$$d_{ij}^{\mathrm{smooth}}(R) = \begin{cases} 1 & \text{if } x \le r_1 \\ \dfrac{1}{1 + e^{2|r_1 - r_0|/(r_1 - R) - |r_1 - r_0|/(R - r_0)}} & \text{if } r_1 < x < r_0 \\ 0 & \text{if } x \ge r_0 \end{cases} \quad (2)$$

where R is the shortest intermolecular distance between any two atoms in the pair of molecules i and j. For any dimer where the shortest intermolecular separation is less than or equal to r_1, the two-body interaction is treated quantum mechanically ($d^{\text{smooth}} = 1$). If the shortest intermolecular distance is greater than or equal to r_0, it is approximated classically ($d^{\text{smooth}} = 0$). For dimers whose shortest intermolecular separation lies within the damping region between r_1 and r_0, the dimer interaction energy is a linear combination of quantum and classical interactions ($0 < d^{\text{smooth}} < 1$).

2.2. Nature of the Ab Initio Force Field (AIFF) in Periodic Systems. The success of this fragment QM/MM approach depends critically on the quality of the force field used to approximate the long-range two- and the many-body intermolecular interactions. The force field used here includes long-range two-body electrostatics, induction (both many-body and long-range two-body), long-range two-body dispersion, and three-body dispersion:

$$E^{\text{MM}} = E_{\text{es}} + E_{\text{ind}} + E_{2-\text{body disp}} + E_{3-\text{body disp}} \tag{3}$$

Note that the addition of dispersion terms and the incorporation of periodic boundary conditions distinguish this force field from an earlier version.[50]

The force field is parametrized with atom-centered distributed multipole moments, distributed static polarizabilities, and isotropic atomic dispersion coefficients. The isotropic dispersion coefficients are computed from the isotropic frequency-dependent polarizabilities. The multipole moments and polarizabilities are represented in a spherical tensor formalism and can be computed for each monomer in the unit cell.[53] The computational time required to determine these parameters is typically small compared to the time required to evaluate the QM interactions in the system.

The force field also requires short-range induction and dispersion damping function parameters which are unfortunately more difficult to obtain from first principles. As described below, the damping parameters are obtained empirically. The following sections describe each of the force-field terms in greater detail.

The following notation is used below: The letters A, B, and C refer to molecules, while a, b, and c refer to atoms in those molecules. The letters t and u refer to spherical tensor components of the multipole moments/polarizabilities.

2.2.1. Long-Range Two-Body Electrostatics. The force fields adopts a distributed multipole representation of the interacting molecular charge densities.[54−56] Heavy atom densities are represented with a rank 4 expansion (up to hexadecapole moments), while hydrogen atoms include up to rank 2 (quadrupole moments). As described in ref 53, the interaction between two molecules A and B is given by

$$E_{\text{es}}^{\text{AB}} = \sum_{a \in \text{A}} \sum_{b \in \text{B}} \sum_{tu} Q_t^a T_{tu}^{ab} Q_u^b \tag{4}$$

where Q_t^a represents the t-th multipole moment component on atom a, and T_{tu}^{ab} contains the distance and orientation dependence of the interaction (the multipole moments are generally anisotropic and are typically represented in a local molecular coordinate system). Using real spherical tensors, t and u run over the 25 rank 4 components: charge ($t = 00$), dipole ($t = 10, 11c, 11s$), quadrupole ($t = 20, 21c, 21s, 22c, 22s$), octopole ($t = 30, 31c, 31s, 32c, 32s, 33c, 33s$), and hexadecapole ($t = 40, 41c, 41s, 42c, 42s, 43c, 43s, 44c, 44s$) moments. Electrostatic interactions up to R^{-5} are included in eq 4.

Calculating the electrostatics for an infinite crystal formally requires a lattice summation between each of the central unit cell molecules A and all other molecules B, including an infinite number of periodic images:

$$E_{\text{es}}^{\text{lattice}} = \sum_{\text{A}} \sum_{\text{B} \neq \text{A}} E_{\text{es}}^{\text{AB}} \tag{5}$$

We evaluate this expression via multipolar Ewald summation, drawing heavily from ref 57. The resulting total two-body lattice interaction energy is given by

$$\begin{aligned} E_{\text{es}}^{\text{lattice}} = & \sum_{\text{A}} \sum_{\text{B} \neq \text{A}} \sum_{N} \sum_{ab} \sum_{tu} Q_t^a (\mathscr{T}_{tu}^{ab} + \tilde{\mathscr{T}}_{tu}^{ab}) Q_u^b \\ & - \frac{\gamma}{\sqrt{\pi}} \sum_{\text{A}} \sum_{a} (Q_{00}^a)^2 - \sum_{\text{A}} \sum_{a} \sum_{a' \neq a} \sum_{tu} Q_t^a T_{tu}^{aa'} Q_u^{a'} \\ & + \sum_{\text{A}} \sum_{\text{B} \neq \text{A}} \sum_{ab} \sum_{t+u=2} Q_t^a \mathscr{T}_{tu}^{ab} Q_u^b \end{aligned} \tag{6}$$

where N refers to the image cell index in the Ewald summation. In the first term of this equation, the $\tilde{\mathscr{T}}_{tu}^{ab}$ and $\mathscr{T}_{tu}^{ab}$ are the interaction functions in direct and reciprocal space, respectively. $\mathscr{T}_{tu}^{ab}$ and $\tilde{\mathscr{T}}_{tu}^{ab}$ are analogous to the T_{tu}^{ab} terms in eq 4 but with extra components arising from the Ewald summation. They include the orientation dependence between site−site vectors and lattice vectors in direct and reciprocal space, the site−site distance dependence, and the coefficient that controls the length scales in the direct and reciprocal space portions Ewald summation. Explicit expressions for $\tilde{\mathscr{T}}_{tu}^{ab}$ and $\tilde{\mathscr{T}}_{tu}^{ab}$ are given in the Supporting Information.

The first term in eq 6 gives the basic Ewald summation in direct and reciprocal space. However, the Ewald method introduces a self-interaction energy (i.e., the interaction of an atomic site with itself, A = B and $a = b$), which is explicitly subtracted out by the second term in eq 6. Only the charge−charge self-interaction term needs to be corrected for in a spherical harmonic formulation.[57] The Ewald sum here also includes terms corresponding to interactions between pairs of atoms within a single molecule. These unwanted intramolecular electrostatic terms are eliminated by the third term. Finally, the fourth term corresponds to a boundary condition term for interactions with total multipole moment of two (dipole−dipole and charge−quadrupole interactions). Boundary condition terms with total multipole moment less than two, which correspond to a crystal shape-dependent surface contribution in polar/ionic crystals, are omitted in this formulation (i.e., tinfoil boundary conditions are adopted). See ref 57 and references cited therein for details. In practice, we perform the Ewald sum on the total multipole moments (permanent plus induced), as described below.

2.2.2. Induction. Many-body induction can also be important in determining molecular crystal structures and energetics, especially when the crystals contain polar molecules and/or hydrogen bonds.[58] For this reason, the force field includes self-consistent induction for both long-range two-body interactions (relatively unimportant) and many-body interactions (important).

Multipole moments on nearby molecules B induce multipole moments ΔQ_t^a on atom a in molecule A:

$$\Delta Q_t^a = - \sum_{\text{B} \neq \text{A}} \sum_{b} \sum_{a'} \sum_{t'u} \alpha_{tt'}^{aa'} f_n(R,\beta) T_{t'u}^{a'b} (Q_u^b + \Delta Q_u^b) \tag{7}$$

where $\alpha_{tt'}^{aa'}$ is the polarizability of atom a and $f_n(R,\beta)$ is a short-range electrostatic damping function. We typically compute

atom-centered distributed polarizabilities up to rank 2 (quadrupole−quadrupole) on heavy atoms and up to rank 1 (dipole−dipole) on hydrogen atoms.[59,60] The distributed polarizabilities are computed according to the Williams−Stone−Misquitta procedure.[61,62]

Of course, the multipole moments on molecule A also induce multipole moments ΔQ_u^b on the atoms in molecule B. Thus, eq 7 must be iterated to self-consistency on all atoms. We iterate the induced multipole moments until the energy converges to 10^{-5} kJ/mol. The final induction energy, which includes many-body induction, is given by

$$E_{\text{ind}} = \frac{1}{2}\sum_{\text{A}}\sum_{\text{B}\neq\text{A}} \Delta Q_t^a f_n(R,\beta) T_{t'u}^{a'b} Q_u^b \tag{8}$$

We apply the Tang−Toennies damping function $f_n(R,\beta)$:

$$f_n(R,\beta) = 1 - \sum_{k=0}^{n}\left(\frac{(\beta R)^k}{k!}\right)e^{-\beta R} \tag{9}$$

The subscript n in $f_n(R,\beta)$ refers to the order of the electrostatic interaction R^{-n} in $T_{t'u}^{a'b}$. The constant β is determined empirically for each type of molecule, as described previously.[50]

Generalizing this treatment of many-body induction to infinite periodic systems with high-order multipoles is complicated by two key issues. First, we need to determine the self-consistent induced moments in the context of an infinite lattice. In principle, the iteration of the induced moments to self-consistency could be coupled with the Ewald summation for the permanent electrostatics. Although that is conceptually straightforward, the complexity of the multipolar Ewald summation makes it messy in practice. Furthermore, it is unnecessary: distant molecules do not contribute significantly to the induced multipole moments in the central unit cell. They will, however, induce multipole moments on other molecules which are closer to the central unit cell and therefore interact in a many-body fashion.

Therefore, we evaluate the induced multipole moments in a finite cluster that is large enough to capture these effects. In practice, we find that including all molecules within 25 Å of the central unit cell molecules converges the induced multipole moments to within 0.001 au. At each iteration, we evaluate only the induced moments on the molecules in the central unit cell. Induction effects between groups of molecules outside the central unit cell are not included. Rather, the induced moments on the periodic image molecules are then set equal to those of the reference central cell molecules, mimicking the infinite crystal. This process is repeated until the induced moments reach self-consistency.

The use of a finite cluster introduces slight asymmetries in the induced moments on symmetry-equivalent atoms, with the induced multipole moments typically varying by a few percent or less. The larger the finite cluster, the smaller the errors. In principle, these errors could be eliminated entirely through a proper treatment of space group symmetry, though we do not do so here.

Second, the induction interactions must be damped at short-range to avoid the "polarization catastrophe," particularly when evaluating the many-body induction terms. Damping is trivial to apply when determining the multipole moments in a finite cluster, but again it complicates the Ewald summation equations. Here, we include it by recognizing that damping is important only within short ranges (<10 Å). We perform the Ewald sum using undamped interaction energies and then correct the resulting induction energy with the difference between the damped and undamped interactions in the finite cluster used above to determine the induced multipole moments. As long as the finite cluster is larger than the length scale on which the damping function operates, this approach introduces no additional errors.

To summarize, this approach for computing the induction energy in infinite periodic systems has four steps that can be implemented easily:

1. Determine the self-consistent induced multipole moments on all atoms in the central unit cell by interacting them with a finite number of periodic image molecules (a "cluster"). Short-range damping is applied while iterating to self-consistency. Compute the damped induction energy for the central unit-cell molecules interacting with this finite cluster, $E_{\text{ind}}^{\text{cluster}}(\text{damped})$.
2. Use the converged induced multipole moments from step 1 to compute the induction energy without short-range damping, $E_{\text{ind}}^{\text{cluster}}(\text{undamped})$ (i.e., eq 8 with $f_n = 1$). Compute the correction due to short-range damping $\delta E_{\text{damp}}^{\text{cluster}} = E_{\text{ind}}^{\text{cluster}}(\text{damped}) - E_{\text{ind}}^{\text{cluster}}(\text{undamped})$.
3. Replace the permanent multipole moments in eq 6 with the total multipole moments (permanent plus induced) and evaluate the total lattice energy, $E_{\text{es+ind}}^{\text{lattice}}(\text{undamped})$.
4. Correct the total lattice energy for short-range induction damping:

$$E_{\text{es+ind}}^{\text{lattice}}(\text{damped}) = E_{\text{es+ind}}^{\text{lattice}}(\text{undamped}) + \delta E_{\text{damp}}^{\text{cluster}} \tag{10}$$

Our strategy differs moderately from the one in ref 7, but the two approaches probably give similar results. The computational cost of this approach is small compared to the cost of the quantum mechanical calculations in the hybrid fragment model.

2.2.3. Long-Range Two-Body Dispersion. Two-body van der Waals dispersion makes an important contribution to molecular crystals, but the bulk of this interaction is typically captured in the QM portion of the fragment model. Nevertheless, we include two-body dispersion in the force-field to capture the long-range contributions that are missed in the short-range QM treatment.

Two-body dispersion is included in the force-field using isotropic atomic C_6 and C_8 dispersion coefficients:

$$E_{\text{2-body disp}} = -\sum_{\text{A}}\sum_{\text{B}\neq\text{A}}\sum_{a}\sum_{b}\left(f_6\frac{C_6^{ab}}{R_{ab}^6} + f_8\frac{C_8^{ab}}{R_{ab}^8} + \cdots\right) \tag{11}$$

where the f_n are again Tang−Toennies damping functions (eq 9). The damping parameter β in $f_n(R,\beta)$ is determined empirically from atomic van der Waals radii.[63] In this case, the damping function is fairly unimportant, since the force field is used only to describe long-range dispersion. The lattice sum is evaluated explicitly with a large cutoff (e.g., 15 or 20 Å).

The dispersion coefficients C_n^{ab} for atoms a and b (in atomic units) are determined via Casimir−Polder integration over the isotropic frequency-dependent polarizabilities:[53]

$$C_6^{ab} = \frac{3}{\pi}\int_0^\infty \alpha_{11}^a(i\nu)\alpha_{11}^b(i\nu)\,\mathrm{d}\nu \tag{12}$$

$$C_8^{ab} = \frac{15}{2\pi}\left(\int_0^\infty \alpha_{11}^a(i\nu)\alpha_{22}^b(i\nu)\,\mathrm{d}\nu + \int_0^\infty \alpha_{22}^a(i\nu)\alpha_{11}^b(i\nu)\,\mathrm{d}\nu\right) \tag{13}$$

where α_{11} and α_{22} are the isotropic dipole−dipole and quadrupole−quadrupole frequency-dependent polarizabilities, respectively. Note that for a given geometry, the frequency-dependent polarizabilities need only be determined once for each atom in the unit cell. The dispersion coefficients and interaction energy between any pair of atoms can then be computed quickly by performing the one-dimensional integral over imaginary frequency.

The Casimir−Polder integral is evaluated via 10-point Gauss−Legendre quadrature after performing a change of variables that maps v to t according to $v = v_0(1 + t)/(1 - t)$, with $v_0 = 0.5$.[64] This transformation converts the semi-infinite integral to one between −1 and 1.

2.2.4. Three-Body Dispersion. Many-body dispersion is usually expected to be small compared to other intermolecular interactions, and it is often neglected in molecular crystal calculations. However, the leading many-body contribution, three-body Axilrod−Teller−Muto dispersion, makes a significant contribution in crystals containing nonpolar molecules, such as in benzene[65] or rare gases.[66] As we demonstrate below, it can also contribute nontrivially to the lattice energy of even some polar, hydrogen-bonded molecular crystals. The magnitude of the three-body dispersion contribution depends strongly on the orientation of the interacting bodies,[65] and it can be important for discriminating between putative crystal polymorphs.[63]

The AIFF incorporates the Axilrod−Teller−Muto triple-dipole three-body intermolecular dispersion term.[67,68] For a given set of three molecules ABC, this is given by

$$E^{\mathrm{ABC}}_{\text{3-body disp}} = \sum_{a \in \mathrm{A}} \sum_{b \in \mathrm{B}} \sum_{c \in \mathrm{C}} f_9 C_9^{abc} \frac{(1 + 3\cos\hat{a}\cos\hat{b}\cos\hat{c})}{R_{ab}^3 R_{bc}^3 R_{ac}^3} \tag{14}$$

where C_9^{abc} is the dispersion coefficient for atom triplet abc, R_{ij} is the distance between atoms i and j, and $\hat{a}$, $\hat{b}$, and $\hat{c}$ are the angles of the triangle formed by the three atoms. The damping function f_9 is written as a product of three two-body Tang−Toennies damping functions.[63,69,70]

A similar atom−atom triple-dipole dispersion formulation for molecules has been used, for example, by von Lilienfeld and Tkatchenko.[63] They demonstrated that it reproduces SAPT three-body dispersion energies fairly well. Our implementation differs from theirs primarily in how the C_9 coefficients are obtained. Three-body dispersion corrections based on coupled Kohn−Sham theory, such as the approach used here, are known to predict the asymptotic dispersion contributions accurately.[37,69,71]

The total three-body dispersion contribution of the lattice is given by summing eq 14 over all possible triplets of molecules. Only one of these molecules needs lie in the central unit cell. The other two may either reside in the unit cell or be periodic image molecules. We perform the lattice sum explicitly up to a user-defined cutoff (e.g., 10 Å). In practice, most of the contribution comes from cases with one molecule in the unit cell and the other two outside it. Of course, the details vary with the number and the chemical nature of the molecules in the unit cell.

In the formulation used here, the three atoms a, b, and c lie on different molecules. This means that only the intermolecular three-body dispersion contribution is included. Important interatomic three-body dispersion contributions involving only one or two molecules need to be captured by the QM portion of the model.

The C_9 coefficient can be calculated using Casimir−Polder integration:

$$C_9^{abc} = \frac{3}{\pi}\int_0^\infty \alpha_{11}^a(iv)\alpha_{11}^b(iv)\alpha_{11}^c(iv)\mathrm{d}v \tag{15}$$

or it can be estimated from two-body C_6:

$$C_9^{abc} \approx \frac{2S^aS^bS^c(S^a + S^b + S^c)}{(S^a + S^b)(S^b + S^c)(S^c + S^a)} \tag{16}$$

where $S^a = C_6^{aa}((\alpha_{11}^b(0)\alpha_{11}^c(0))/(\alpha_{11}^a(0)))$ and $\alpha_{11}(0)$ is static dipole−dipole polarizabilities. We tested both approaches on a handful of systems and found that the C_9 coefficients estimated via eq 16 are typically ∼5% larger than those computed from eq 15. Since we already have the frequency-dependent polarizabilities, we adopt eq 15.

This formalism assumes that any important interatomic three-body dispersion terms involving only one or two monomers (between two atoms on one monomer and one on another, for example) are handled in the quantum mechanical two-body interaction terms. Of course, three-body dispersion terms are *not* captured at the MP2 level,[72] in which case one might consider including additional terms.

2.2.5. Terms Not Included in the Force Field. Before discussing the results, it is worth considering some of the terms that are not included in the force field. First, in the two-body case, the force field does not include exchange/repulsion, penetration, and charge-transfer effects. These effects are primarily short-range in nature, so they are handled in the quantum mechanical portion of the model. The absence of these terms from the force-field is therefore expected to be unimportant.

At the many-body level, we only explicitly include some of the most important terms. Many-body induction is performed self-consistently, but many-body dispersion is only approximated via the leading Axilrod−Teller−Muto term. The use of distributed multipolar expansions and asymptotic dispersion interaction formulations is potentially problematic at short ranges, which is where these terms are most important. As described above, empirical damping factors are needed to compensate at short-range. Furthermore, various other many-body terms (exchange, exchange−induction, induction−dispersion, etc.) are not included explicitly.

Despite these issues, the model performs very well, as we demonstrate below. We attribute this success to a combination of fortuitous error cancellation and to the use of empirical damping factors. In particular, the induction damping parameter for each type of intermolecular interaction is determined by fitting the AIFF induction contribution to the MP2 many-body contribution in a small test set of trimers (none of which are taken from the crystal). So it really includes some effect of the other three-body contributions present in MP2.

Finally, we note that one might circumvent some of these issues by using a hybrid of explicit three-body QM calculations (using supermolecular or SAPT approaches) theory at short ranges and the asymptotic expressions at longer ranges.[37] Of course, including any quantum mechanical treatment of trimers would substantially increase the computational cost of the model, especially for larger molecules.

3. COMPUTATIONAL DETAILS

We perform lattice energy calculations for seven different molecular crystals (ice, formamide, acetamide, imidazole, benzene,

ammonia, and carbon dioxide) using a procedure that is analogous to the one used in ref 25. For the first five crystals, the geometries are identical to those used in ref 25. They were optimized under the constraint of frozen experimental lattice parameters with the HMBI method using RI-MP2/aug-cc-pVDZ and the Amoeba force field. The geometries for ammonia and carbon dioxide come from ref 30.

The quantum mechanical calculations were performed using counterpoise-corrected dual basis RI-MP2[73] and the Dunning aug-cc-pVDZ, aug-cc-pVTZ, and aug-cc-pVQZ basis sets[74] for the QM part. Energies at the complete basis set limit were estimated by separately extrapolating the HF and MP2 correlation triple and quadruple-ζ basis results.[75,76] Then, a post-MP2 correction was computed using CCSD(T) and a smaller, practical basis set (typically aug-cc-pVDZ, except aug-cc-pVTZ for ice and 6-31+G*[77,78] for acetamide and benzene). All quantum calculations were performed using a development version of Q-Chem 3.1,[79] except for the CCSD(T) ones, which were performed with PSI3.[80]

For the AIFF, the distributed multipole moments and polarizabilities (both isotropic and anisotropic) were calculated with CamCASP[81] using asymptotically corrected PBE and the Sadlej basis set.[82,83] A single induction damping factor was determined empirically for each unique molecule type by optimizing the many-body induction against MP2 many-body induction in a set of 10 trimers at various configurations, none of which were taken from the crystal structure. The induction damping factors used here are: 1.45 (ice and carbon dioxide), 1.40 (formamide and benzene), and 1.35 (acetamide, ammonia, and imidazole) bohr^{-1}. Further details of this procedure can be found in ref 50.

As in our previous work,[25] the smoothing region that transitions from QM to MM is conservatively set at 9−10 Å, except for water, for which 6−7 Å can be used. Shorter cutoffs may be feasible with the improved force field, but we have not investigated that.

Because each fragment is defined as a single molecule, specification of the crystal for the calculation is straightforward with our software. The geometries are specified in Cartesian coordinates, with atoms grouped by molecule. Separate sections of the input file define the lattice parameters, the QM job parameters, the AIFF property calculation parameters, and the various AIFF force field cutoffs, etc. Our software then automatically creates input files for each job (e.g., Q-Chem and CamCASP), distributes and runs the jobs across a user-defined number of parallel processors, collects the results, evaluates the AIFF contributions, and finally computes the HMBI energy according to eq 1.

Finally, for four of the crystals, we estimated the effect of relaxing the experimental lattice parameters, using the same technique we adopted previously.[25] In particular, we generated a one-dimensional potential energy scan by isotropically scaling the lattice parameters *a*, *b*, and *c* in increments of 1%. For each set of lattice parameters, the atoms in the unit cell were optimized with planewave DFT, as described previously. HMBI single-point energies were computed with dual-basis RI-MP2/aug-cc-pVTZ and the AIFF at each point, and a cubic spline was used to estimate the optimal lattice parameters and the change in the lattice energy. This $\Delta E_{\text{lattice}}^{\text{relax}}$ contribution is added to the calculated lattice energy to obtain our best estimate. As noted previously, DFT cost and convergence issues prevented us from applying this procedure to acetamide. For ammonia and carbon dioxide, a similar procedure was already used to determine the geometries, so we did not repeat it here.[30] Implementation of analytic HMBI lattice gradients is in progress, so we hope to fully optimize the structures in the future.

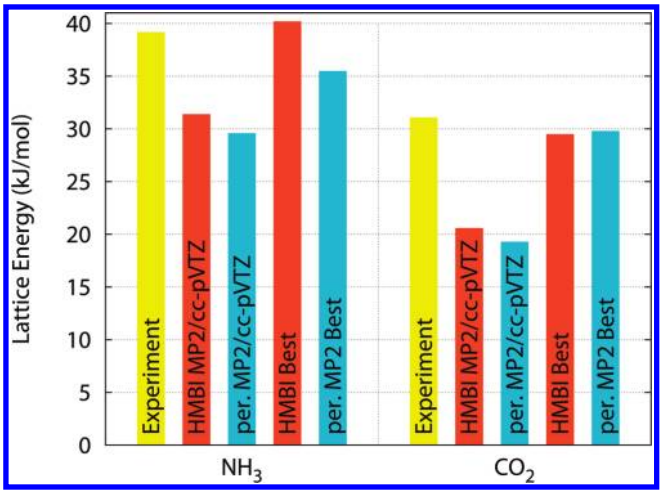

Figure 2. Comparison of HMBI with fully QM periodic MP2 on ammonia and carbon dioxide crystals. Results are presented for both models in the cc-pVTZ basis. We also present our best prediction (complete-basis MP2 + $\Delta^{\text{CCSD(T)}}$) and the largest basis MP2 results from ref 30.

4. RESULTS AND DISCUSSION

The performance of the HMBI model for molecular crystals will be evaluated in two ways: First, to gauge the quality of the AIFF approximation, we examine how faithfully the QM/MM approach used here reproduces fully QM results. Specifically, we compare with benchmark periodic local MP2 lattice energy predictions for the ammonia and carbon dioxide crystals. Second, we determine how accurately molecular crystal lattice energies can be predicted compared to experiment for seven different molecular crystals. Finally, we decompose the different force field contributions to identify the important interactions. We find that three-body dispersion interactions are surprisingly important in a number of cases, even in some hydrogen-bonded molecular crystals where induction would be expected to dominate.

4.1. Comparison with Local Periodic MP2 Lattice Energies.

As mentioned in the Introduction Section, periodic local MP2 calculations on small-molecule organic crystals are now feasible. Those calculations enable the benchmarking of the HMBI approach with a fully QM treatment. We examine two molecular crystals for which large-basis periodic MP2 results exist: ammonia and carbon dioxide.[30]

To match the results of ref 30 as closely as possible, we performed HMBI calculations using local TRIM-MP2[84] with the identical cc-pVTZ basis set and crystal structure. Their periodic MP2 calculations use a different (Saebø−Pulay style)[85] local MP2 approximation, but both models should perform similarly for individual intermolecular interactions. For the purposes of this comparison, we also omit the AIFF three-body dispersion terms, which are not present in MP2 (they first appear in MP3).[72]

As shown in Figure 2, the HMBI model reproduces the full MP2 results well: The predicted lattice energies for NH_3 and CO_2 differ by only 1.8 and 1.3 kJ/mol, respectively from the periodic MP2 results. The error introduced into the predicted lattice energies by these two crystals by the HMBI fragment approach is similar to or smaller than the difference between canonical and local MP2 in the QM portion of our model!

Table 1. HMBI-Predicted Crystal Lattice Energies (kJ/mol)

QM level	ice	formamide	acetamide	imidazole	benzene	NH_3	CO_2
DB-RI-MP2/aug-cc-pVDZ	52.8	70.1	72.2	96.4	60.7	33.4	22.1
DB-RI-MP2/aug-cc-pVTZ	56.7	74.9	76.6	100.2	60.6	37.2	26.1
DB-RI-MP2/aug-cc-pVQZ	58.3	76.7	78.4	100.8	62.8	38.4	27.9
DB-RI-MP2/CBS	59.9	78.6	79.8	102.8	61.6	39.3	29.1
$\Delta^{CCSD(T)}$[a]	0.4	1.8	−0.1	−14.2	−10.4	0.9	0.3
DB-RI-MP2/CBS + $\Delta^{CCSD(T)}$	60.2	80.4	79.7	88.6	51.2	40.2	29.5
est. lattice param. relax., $\Delta E_{lattice}^{relax}$	0.2	0.0		2.2	2.8		
est. change in lattice parameters	−0.9%	−0.3%		−2.6%	−3.4%		
best estimate[b]	60.4	80.4	79.7	90.8	54.0	40.2	29.5
experiment	59	82 ± 0.3[c]	86 ± 2[c]	91 ± 4[c]	52 ± 3[c]	39[d]	31[e]

[a] Post-MP2 correction, $\Delta^{CCSD(T)} = E_{lattice}^{CCSD(T)} - E_{lattice}^{MP2}$, using the basis sets described in the text. [b] Best estimate = $E^{DB-RI-MP2/CBS} + \Delta^{CCSD(T)} + \Delta E_{lattice}^{relax}$. [c] Reported errors are the standard deviation among the set of extrapolated 0 K lattice energies. Actual experimental errors may be larger. See ref 25. [d] See Supporting Information. [e] From ref 30.

We can also compare our predicted HF lattice energy in the same basis with the fully periodic HF value. In this case, we omit all dispersion terms from the AIFF and reoptimized the AIFF induction damping factor using a set of trimer many-body energies at the HF level instead of the MP2 level. The latter step is unimportant for carbon dioxide, which exhibits minimal many-body induction, but the smaller parameter of β = 1.20 $bohr^{-1}$ improves the HF prediction by almost 1 kJ/mol.

Compared with periodic HF, HMBI overestimates the ammonia lattice energy by 1.7 kJ/mol, while the carbon dioxide lattice energies are identical.[30] The fact that the AIFF induction damping factor differs between HF and MP2 supports the idea mentioned in Section 2.2.5 that the empirical damping factor incorporates some of the missing many-body effects into the AIFF induction term.

The good agreement between HMBI and the periodic models can also be partially attributed to the fact that the force field contributions to these crystal energies are rather small: −3.6 and −0.5 kJ/mol for NH_3 and CO_2, respectively, when three-body dispersion is neglected. In both cases, repulsive three-body dispersion would add roughly +1 kJ/mol to the total energy. In any case, the force field captures the long-range and many-body interactions fairly accurately. Furthermore, the HMBI fragment approach is much less computationally expensive than periodic MP2. On the other hand, the fragment approach used here assumes that the crystal can be partitioned into separate molecular fragments, which is not always true (e.g., polynitrogen crystals).[86]

4.2. Comparison with Experimental Lattice Energies. Having demonstrated that the HMBI fragment model nearly reproduces fully quantum mechanical results, the next step is to determine how accurately such predictions reproduce experimental lattice energies. We have already demonstrated that HMBI with the Amoeba force field reproduces lattice energies to within 4−5 kJ/mol on 5 molecular crystals: ice, formamide, acetamide, imidazole, and benzene.[25] Here, we revisit those crystals with the improved force field, and we also add ammonia and carbon dioxide to the test set. These seven crystals include a representative range of intermolecular interactions, ranging from hydrogen bonding (ice, formamide, acetamide, and ammonia) to dispersion (benzene, carbon dioxide) or both (imidazole). For carbon dioxide, we use the experimental lattice energy quoted in ref 30. For ammonia, we use a revised version of the lattice energy cited in ref 30 in which we have made an improved estimate of the zero-point energy contribution. See the Supporting Information for details. For the other five, we use our earlier estimates for the experimental lattice energy.[25]

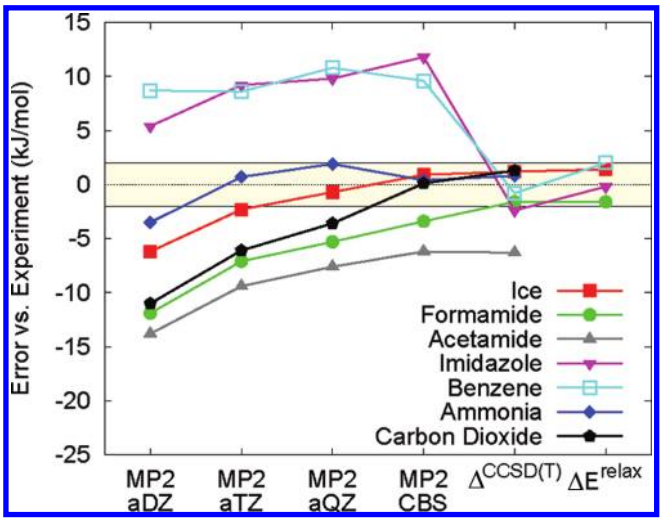

Figure 3. Convergence of the predicted lattice energies toward the experimental values. The yellow band highlights an error of ±2 kJ/mol.

The calculated lattice energies are listed in Table 1 and plotted as errors relative to experiment in Figure 3. Bear in mind that the experimental lattice energies themselves are probably in error by a couple kJ/mol or more.[25,87,88] Increasing the quality of the wave function used for the QM calculations systematically converges the predicted HMBI lattice energies toward the experimental values. Post-MP2 correlation, $\Delta^{CCSD(T)}$, is particularly important for benzene and imidazole.[25] The estimated lattice parameter relaxation effects, $\Delta E_{lattice}^{relax}$, are small, with the largest shift of 2.8 kJ/mol coming from benzene. The estimated change in the lattice parameters is also mostly small. The largest change occurs for benzene, where the parameters shrink by an estimated 3.4%. Overall, in six of the seven cases, our best HMBI lattice energy prediction lies within 2 kJ/mol of the experimental value, which is on par with typical experimental errors!

These lattice energy predictions compare favorably with the other calculations found in the literature that have been summarized in ref 25. For example, periodic density functional theory predictions with empirical dispersion corrections often predict

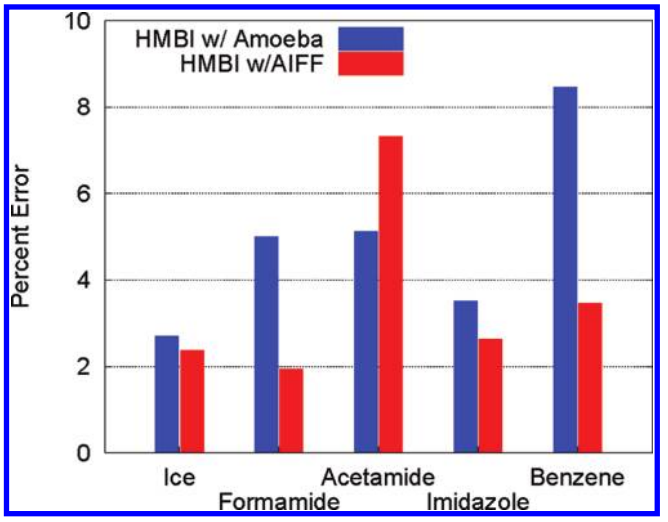

Figure 4. Comparison of the percent errors in the best estimate HMBI lattice energy predictions for the Amoeba and AIFF force fields.

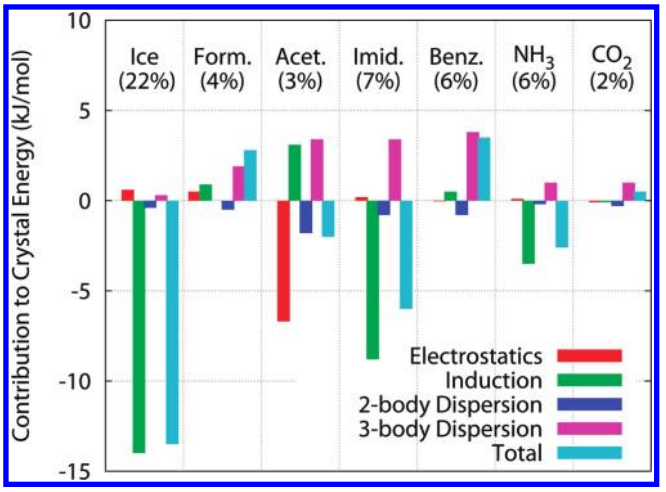

Figure 5. Ab initio force field contributions per molecule to the total crystal energy of the seven crystals considered. The numbers in parentheses indicate the fraction of the net force field contribution relative to the total lattice energy. Note that attractive (negative) contributions increase the lattice energy, while repulsive (positive) ones decrease it.

lattice energies with errors ranging from a couple kJ/mol to several times larger than that. For NH_3 and CO_2, the 1−2 kJ/mol errors in our best predictions are comparable to or better than the best periodic MP2 predictions.

For additional perspective, consider that relative energy differences between closely spaced molecular crystal polymorphs are often on the order of ∼1 kJ/mol. One anticipates some degree of error cancellation between the "absolute" lattice energies when comparing relative polymorph energies. Thus, the ability to predict lattice energies to ∼2 kJ/mol bodes well for the possibility of reliably distinguishing between crystal polymorphs.

For all of the cases for which Amoeba is parametrized, except acetamide, the AIFF reduces the error in the predicted lattice energy, as shown in Figure 4. On the other hand, the 6 kJ/mol error for the best acetamide prediction is much worse than those for the other crystals. In fact, the use of the AIFF increases the error in the predicted lattice energy slightly compared to the Amoeba force field. The reasons for this behavior are unclear, but the predictions underestimate the experimental lattice energy for acetamide. Relaxing the experimental lattice parameters would increase the calculated lattice energy and potentially improve the prediction. Implementation of analytical derivatives of the AIFF and crystal lattice derivatives is in progress, so we hope to investigate this possibility in the near future. Alternatively, perhaps larger-basis $\Delta^{CCSD(T)}$ correlation corrections are needed. The large size of the acetamide unit cell (18 monomers, 162 atoms, and 1008 significant dimers without symmetry) limited the CCSD(T) calculations to the small 6-31+G* basis. Finally, another source of error might be the moderately small aug-cc-pVDZ basis used in optimizing the crystal structure. The degree of pyramidalization in NH_2 groups can be quite sensitive to the electronic structure treatment, for example.

4.3. Analysis of the Ab Initio Force Field Contributions. Finally, we examine the AIFF contributions in more detail. As shown in Figure 4 the AIFF significantly improves upon Amoeba for capturing the long-range and many-body contributions. To provide further insight into this behavior, Figure 5 decomposes the AIFF energy into its individual contributions: long-range two-body electrostatic, induction (both long-range two- and three-body), long-range two-body dispersion, and three-body dispersion.

The electrostatics and induction terms provide a major contribution to the force field energy, particularly for hydrogen-bonded crystals like ice or ammonia. The importance of induction to describing hydrogen-bond cooperativity and organic crystals is well-known.[58,89]

On the other hand, the long-range two-body dispersion terms in the force field contribute very little in all cases. This does not mean that total two-body dispersion is unimportant. Rather, the important two-body dispersion contributions occur at shorter ranges and are captured in the QM part of the model. The fact that the force field dispersion terms only describe long-range contributions means that the C_6 term (R^{-6} decay) is much more important than the C_8 term (R^{-8} decay). In the cases examined here, C_6 provides 97−99% of the total long-range dispersion, while the C_8 coefficient contributes the remaining 1−3%. The C_{10} contributions are yet another order of magniture smaller, so they are not included.

The contribution of three-body Axilrod−Teller−Muto dispersion is particularly interesting. Conventional wisdom would argue that many-body dispersion is only significant in nonpolar/aromatic species, where induction is unimportant. For this reason, its contribution is often ignored in systems containing polar or hydrogen-bonded molecules.

As expected, three-body dispersion contributes significantly for benzene, imidazole, and carbon dioxide, while its contribution is negligiable for ice. For the benzene crystal structure used here, for example, the repulsive three-body dispersion term contributes 4.6 kJ/mol. This is fairly similar to the SAPT(DFT) result of 6.5 kJ/mol for the benzene crystal at the experimental geometry.[37]

Contrary to conventional wisdom, however, we observe that even for the hydrogen-bonded formamide and acetamide crystals, three-body dispersion contributes several kJ/mol to the overall lattice energy. More importantly, it is similar to or larger in magnitude than the induction contribution! Combining these results with the evidence that three-body dispersion can be important in ranking different crystal polymorphs[63] suggests that the many-body dispersion may be more important than has often been thought. Further study is clearly needed.

Together, the inclusion of three-body dispersion and the improved treatment of induction account for most of the differences between the results with the Amoeba and ab initio force fields. The long-range two-body electrostatics and dispersion contributions in the two force fields typically differ by much less than 1 kJ/mol.

The need to determine the AIFF parameters on-the-fly obviously makes the AIFF much more computationally expensive than Amoeba or other conventional force fields. On the other hand, the force field parameters are evaluated separately for each monomer in the central unit cell, so the number of parameters that need to be computed grows only linearly with the number of molecules in the unit cell. Trivial parallelization of the computational effort can be achieved easily by calculating the AIFF parameters for each monomer on a separate processor. The computational cost of evaluating these monomer properties is small compared to the cost of the calculating many high-level QM dimer interaction energies. Overall, these AIFF-based crystal calculations are not significantly more expensive than the Amoeba-based ones for which timings have been reported previously.[25]

5. CONCLUSIONS

In summary, the HMBI fragment QM/MM model used here provides an accurate and computationally affordable means of predicting molecular crystal lattice energies. In particular, we have demonstrated that a polarizable force field based on distributed multipoles, distributed polarizabilities, and atomic dispersion coefficients which are calculated on-the-fly from DFT provides an accurate treatment of long-range two-body and many-body interactions.

For two different crystals, the model reproduces periodic MP2 results to within a couple kJ/mol. It also predicts six of the seven crystal lattice energies examined to within experimental error. The ability to systematically improve the predictions along with the standard hierarchy of conventional electronic structure methods and basis sets is critical to achieving these high accuracies.

The favorable computational scaling inherent to fragment methods makes it feasibly to apply such high-level electronic structure methods to molecular crystals. In particular, the approximation of long-range and many-body intermolecular interactions using a polarizable force field makes the model described here linear scaling for all unit-cell sizes. Furthermore, fragment methods are naturally suited for massively parallel computing, and very high efficiencies can be obtained with hundreds or more processors.

All of these features make this approach very promising for molecular crystal structure prediction. Future work will focus on implementing nuclear gradients of this improved force field that will enable full crystal structure optimization. Other computational speed-ups could be obtained by exploiting crystal space group symmetry and by new developments in accurate, low-cost electronic structure methods.

■ ASSOCIATED CONTENT

Supporting Information. More detailed expressions for the Ewald summation intermediates and discussion of the ammonia lattice energy are provided. This material is available free of charge via the Internet at http://pubs.acs.org.

■ AUTHOR INFORMATION

Corresponding Author
*E-mail: gregory.beran@ucr.edu.

■ ACKNOWLEDGMENT

Financial support from the National Science Foundation (CHE-1112568) and supercomputer time from the Teragrid (TG-CHE090099 and TG-CHE110064) are gratefully acknowledged. The authors also thank Alston Misquitta and Anthony Stone for providing their CamCASP software and for helpful discussions on its use, and Lorenzo Maschio and co-workers for providing their optimized crystal structures for ammonia and carbon dioxide.

■ REFERENCES

(1) Price, S. L. *Acc. Chem. Res.* **2009**, *42*, 117–26.
(2) Haas, S.; et al. *Phys. Rev. B* **2007**, *76*, 115203.
(3) Bauer, J.; Spanton, S.; Quick, R.; Quick, J.; Dziki, W.; Porter, W.; Morris, J. *Pharm. Res.* **2001**, *18*, 859–866.
(4) Day, G. M.; et al. *Acta Cryst. B* **2009**, *65*, 107–125.
(5) Kazantsev, A. V.; Karamertzanis, P. G.; Adjiman, C. S.; Pantelides, C. C.; Price, S. L.; Galek, P. T. a.; Day, G. M.; Cruz-Cabeza, A. J. *Int. J. Pharm.* **2011**, *418*, 168–178.
(6) Price, S. L. *Int. Rev. Phys. Chem.* **2008**, *27*, 541–568.
(7) Price, S. L.; Leslie, M.; Welch, G. W. A.; M. Habgood, L. S. P.; Karamertzanis, P. G.; Day, G. M. *Phys. Chem. Chem. Phys.* **2010**, *12*, 8478–8490.
(8) Li, T.; Feng, S. *Pharm. Res.* **2006**, *23*, 2326–2332.
(9) Kleis, J.; Lundqvist, B. I.; Langreth, D. C.; Schröder, E. *Phys. Rev. B* **2007**, *76*, 1002001.
(10) Neumann, M. A.; Perrin, M. A. *J. Phys. Chem. B* **2005**, *109*, 15531–15541.
(11) Neumann, M. A.; Leusen, F. J. J.; Kendrick, J. *Angew. Chem., Int. Ed.* **2008**, *47*, 2427–2430.
(12) Civalleri, B.; Zicovich-Wilson, C. M.; Valenzano, L.; Ugliengo, P. *CrystEngComm* **2008**, *10*, 405–410.
(13) Karamertzanis, P. G.; Day, G. M.; Welch, G. W. A.; Kendrick, J.; Leusen, F. J. J.; Neumann, M. A.; Price, S. L. *J. Chem. Phys.* **2008**, *128*, 244708.
(14) Sorescu, D. C.; Rice, B. M. *J. Phys. Chem. C* **2010**, *114*, 6734–6748.
(15) Balu, R.; Byrd, E. F. C.; Rice, B. M. *J. Phys. Chem. B* **2011**, *115*, 803–10.
(16) Shimojo, F.; Wu, Z.; Nakano, A.; Kalia, R. K.; Vashishta, P. *J. Chem. Phys.* **2010**, *132*, 094106.
(17) Kristyan, S.; Pulay, P. *Chem. Phys. Lett.* **1994**, *229*, 175–180.
(18) Riley, K. E.; Pitonák, M.; Jurecka, P.; Hobza, P. *Chem. Rev.* **2010**, *110*, 5023–63.
(19) Grimme, S. *J. Comput. Chem.* **2004**, *25*, 1463–1473.
(20) Lu, D.; Li, Y.; Rocca, D.; Galli, G. *Phys. Rev. Lett.* **2009**, *102*, 206411.
(21) Li, Y.; Lu, D.; Nguyen, H.-V.; Galli, G. *J. Phys. Chem. A* **2010**, *114*, 1944–1952.
(22) Dion, M.; Rydberg, H.; Schröder, E.; Langreth, D. C.; Lundqvist, B. I. *Phys. Rev. Lett.* **2004**, *92*, 246401.
(23) Thonhauser, T.; Cooper, V. R.; Li, S.; Puzder, A.; Hyldgaard, P.; Langreth, D. C. *Phys. Rev. B* **2007**, *76*, 125112.
(24) Hongo, K.; Watson, M. A.; Sanchez-Carrera, R. S.; Iitaka, T.; Aspuru-Guzik, A. *J. Phys. Chem. Lett.* **2010**, *1*, 1789–1794.
(25) Beran, G. J. O.; Nanda, K. *J. Phys. Chem. Lett.* **2010**, *1*, 3480–3487.
(26) Rivera, S. A.; Allis, D. G.; Hudson, B. S. *Cryst. Growth Des.* **2008**, *8*, 3905–3907.
(27) Usvyat, D.; Maschio, L.; Manby, F. R.; Casassa, S.; Pisani, C.; Schütz, M. *Phys. Rev. B* **2007**, *76*, 075102.
(28) Pisani, C.; Maschio, L.; Casassa, S.; Halo, M.; Schütz, M.; Usvyat, D. *J. Comput. Chem.* **2008**, *29*, 2113–2124.
(29) Erba, A.; Pisani, C.; Casassa, S.; Maschio, L.; Schütz, M.; Usvyat, D. *Phys. Rev. B* **2010**, *81*, 165108.

(30) Maschio, L.; Usvyat, D.; Schütz, M.; Civalleri, B. *J. Chem. Phys.* **2010**, *132*, 134706.
(31) Usvyat, D.; Civalleri, B.; Maschio, L.; Dovesi, R.; Pisani, C.; Schutz, M. *J. Chem. Phys.* **2011**, *134*, 214105.
(32) Marsman, M.; Grueneis, A.; Paier, J.; Kresse, G. *J. Chem. Phys.* **2009**, *130*, 184103.
(33) Manby, F. R.; Alfe, D.; Gillan, M. J. *Phys. Chem. Chem. Phys.* **2006**, *8*, 5178–5180.
(34) Addicoat, M. a.; Collins, M. a. *J. Chem. Phys.* **2009**, *131*, 104103.
(35) Fedorov, D. G.; Kitaura, K. *J. Phys. Chem. A* **2007**, *111*, 6904–6914.
(36) Podeszwa, R.; Bukowski, R.; Rice, B. M.; Szalewicz, K. *Phys. Chem. Chem. Phys.* **2007**, *9*, 5561–5569.
(37) Podeszwa, R.; Rice, B. M.; Szalewicz, K. *Phys. Rev. Lett.* **2008**, *101*, 115503.
(38) Nagayoshi, K.; Ikeda, T.; Kitaura, K.; Nagase, S. *J. Theory Comput. Chem.* **2003**, *2*, 233–244.
(39) Hirata, S. *J. Chem. Phys.* **2008**, *129*, 204104.
(40) Sode, O.; Keceli, M.; Hirata, S.; Yagi, K. *Int. J. Quantum Chem.* **2009**, *109*, 1928–1939.
(41) Dahlke, E. E.; Truhlar, D. G. *J. Phys. Chem. B* **2006**, *3*, 10595–10601.
(42) Dahlke, E. E.; Truhlar, D. G. *J. Chem. Theory Comput.* **2007**, *3*, 46–53.
(43) Nagata, T.; Brorsen, K.; Fedorov, D. G.; Kitaura, K.; Gordon, M. S. *J. Chem. Phys.* **2011**, *134*, 124115.
(44) Tschumper, G. S. *Chem. Phys. Lett.* **2006**, *427*, 185–191.
(45) Dahlke, E. E.; Truhlar, D. G. *J. Chem. Theory Comput.* **2007**, *3*, 1342–1348.
(46) Stoll, H.; Paulus, B.; Fulde, P. *J. Chem. Phys.* **2005**, *123*, 144108.
(47) Hermann, A.; Schwerdtfeger, P. *Phys. Rev. Lett.* **2008**, *101*, 183005.
(48) Bludsky, O.; Rubes, M.; Soldan, P. *Phys. Rev. B* **2008**, *77*, 092103.
(49) Beran, G. J. O. *J. Chem. Phys.* **2009**, *130*, 164115.
(50) Sebetci, A.; Beran, G. J. O. *J. Chem. Theory Comput.* **2010**, *6*, 155–167.
(51) Kazantsev, A. V.; Karamertzanis, P. G.; Adjiman, C. S.; Pantelides, C. C. *J. Chem. Theory Comput.* **2011**, *7*, 1998–2016.
(52) Subotnik, J. E.; Sodt, A.; Head-Gordon, M. *J. Chem. Phys.* **2008**, *128*, 034103.
(53) Stone, A. J. *The Theory of Intermolecular Forces*; Clarendon Press: Oxford, U.K., 2002; chpt. 3−4, pp 7−9.
(54) Stone, A. J. *Chem. Phys. Lett.* **1981**, *83*, 233–239.
(55) Stone, A. J.; Alderton, M. *Mol. Phys.* **1985**, *56*, 1047–1064.
(56) Stone, A. J. *J. Chem. Theory Comput.* **2005**, *1*, 1128–1132.
(57) Leslie, M. *Mol. Phys.* **2008**, *106*, 1567–1578.
(58) Welch, G. W. A.; Karamertzanis, P. G.; Misquitta, A. J.; Stone, A. J.; Price, S. L. *J. Chem. Theory Comput.* **2008**, *4*, 522–532.
(59) Stone, A. J.; Misquitta, A. J. *Int. Rev. Phys. Chem.* **2007**, *26*, 193–222.
(60) Welch, G. W. A.; Karamertzanis, P. G.; Misquitta, A. J.; Stone, A. J.; Price, S. L. *J. Chem. Theory Comput.* **2008**, *4*, 522–532.
(61) Misquitta, A. J.; Stone, A. J. *J. Chem. Theory Comput.* **2008**, *4*, 7–18.
(62) Misquitta, A. J.; Stone, A. J.; Price, S. L. *J. Chem. Theory Comput.* **2008**, *4*, 19–32.
(63) von Lilienfeld, O. A.; Tkatchenko, A. *J. Chem. Phys.* **2010**, *132*, 234109.
(64) Misquitta, A.; Stone, A. *Mol. Phys.* **2008**, *106*, 1631–1643.
(65) Podeszwa, R. *J. Phys. Chem. A* **2008**, *112*, 8884–8885.
(66) Schwerdtfeger, P.; Assadollahzadeh, B.; Hermann, A. *Phys. Rev. B* **2010**, *82*, 205111.
(67) Axilrod, P. M.; Teller, E. *J. Chem. Phys.* **1943**, *11*, 299–300.
(68) Muto, Y. *Proc. Phys.-Math. Soc. Jpn.* **1943**, *17*, 629–631.
(69) Lotrich, V. F.; Szalewicz, K. *J. Chem. Phys.* **1997**, *106*, 9688–9702.
(70) Cencek, W.; Jeziorska, M.; Akin-Ojo, O.; Szalewicz, K. *J. Phys. Chem. A* **2007**, *111*, 11311–9.
(71) Podeszwa, R.; Szalewicz, K. *J. Chem. Phys.* **2007**, *126*, 194101.
(72) Chalasinski, G.; Szczesniak, M. M.; Kendall, R. A. *J. Chem. Phys.* **1994**, *101*, 8860–8869.
(73) Steele, R. P.; Distasio, R. A.; Shao, Y.; Kong, J.; Head-Gordon, M. *J. Chem. Phys.* **2006**, *125*, 074108.
(74) Dunning, T. H. *J. Chem. Phys.* **1989**, *90*, 1007–1023.
(75) Karton, A.; Martin, J. M. L. *Theor. Chem. Acc.* **2006**, *115*, 330–333.
(76) Helgaker, T.; Klopper, W.; Koch, H.; Noga, J. *J. Chem. Phys.* **1997**, *106*, 9639–9646.
(77) Hehre, W. J.; Ditchfield, R.; Pople, J. A. *J. Chem. Phys.* **1972**, *56*, 2257–2261.
(78) Hariharan, P. C.; Pople, J. A. *Theor. Chim. Acta* **1973**, *28*, 213–222.
(79) Shao, Y.; et al. *Phys. Chem. Chem. Phys.* **2006**, *8*, 3172–3191.
(80) Crawford, T. D.; Sherrill, C. D.; Valeev, E. F.; Fermann, J. T.; King, R. A.; Leininger, M. L.; Brown, S. T.; Janssen, C. L.; Seidl, E. T.; Kenny, J. P.; Allen, W. D. *J. Comput. Chem.* **2007**, *28*, 1610–1616.
(81) Misquitta, A. J.; Stone, A. J. *CamCASP*, v5.6; University of Cambridge: Cambridge, U.K., 2011; http://www-stone.ch.cam.ac.uk/programs.html. Accessed February 23, 2011.
(82) Sadlej, A. J. *Collect. Czech. Chem. Commun.* **1988**, *53*, 1995–2016.
(83) Sadlej, A. J. *Theor. Chim. Acta* **1991**, *79*, 123–140.
(84) Lee, M. S.; Maslen, P. E.; Head-Gordon, M. *J. Chem. Phys.* **2000**, *112*, 3592–3601.
(85) Saebø, S.; Pulay, P. *Annu. Rev. Phys. Chem.* **1993**, *44*, 213–236.
(86) Erba, A.; Maschio, L.; Salustro, S.; Casassa, S. *J. Chem. Phys.* **2011**, *134*, 074502.
(87) Shipman, L. L.; Burgess, A. W.; Scheraga, H. A. *J. Phys. Chem.* **1976**, *80*, 52–54.
(88) Chickos, J. S.; Acree, W. E. *J. Phys. Chem. Ref. Data* **2002**, *31*, 537–698.
(89) Steiner, T. *Angew. Chem., Int. Ed.* **2002**, *41*, 48–76.